Electronic Supplementary Information

Uncovering the Active Sites and Demonstrating Stable Catalyst for the Cost-Effective Conversion of Ethanol to 1-Butanol

Mond F. Guo,[1,2] Michel J. Gray,[1] Heather Job,[1] Carlos Alvarez-Vasco,[1,2] Senthil Subramaniam,[1,2] Xiao Zhang,[1,2] Libor Kovarik,[3] Vijayakumar Murugesan,[4] Steven Phillips,[1] and Karthikeyan K. Ramasamy[1,5]

[1.] Chemical & Biological Processing Group, Pacific Northwest National Laboratory, Richland, WA 99354, USA.
[2.] Voiland School of Chemical Engineering & Bioengineering Bioproducts, Science & Engineering Laboratory, Washington State University, 2710 Crimson Way, Richland, WA 99354, USA.
[3.] Environmental Molecular Sciences Laboratory, Pacific Northwest National Laboratory, Richland WA 99354, USA.
[4.] Materials Sciences, Pacific Northwest National Laboratory, Richland WA 99354, USA.
[5.] Correspondence and requests for materials should be addressed to K. K. (email: karthi@pnnl.gov).

Table S1. Selected examples of ethanol coupling to higher alcohols in literature

Catalyst	Temp. (K)	Conv. (%)	Yield* (%)	Ref
CuMgAl	573	4.1	1.6	[1, 2]
Mg_xAl_x	573	40.3	22.1	[3]
Ni/Al_2O_3	503	41.0	19.5	[4]
Mg_3Al_1	673	62.0	14.9	[5]
Mg_3FeAlO	573	50.0	10.0	[6]
Mg_3Al_x	623	35.0	14.0	[7]
Mg_3AlO	573	19.0	4.5	[8]
$Cu_{10}Ni_{10}PMO$	600	56.0	22.0	[9]
MgAl	673	22.2	9.67	[10]
Ni-MgAlO	523	18.7	9.1	[11]
$Cu\text{-}CeO_2$	533	67.0	30.0	[12]
Cu-Ce/AC	673	39.1	21.6	[13]
HAP	623	40.0	32.0	[14]
CuAlMgO-P	**598**	23.3	11.37	[15]
YSZ 500	548	24.2	20.1	[16]
$Cu_{10}Ni_{10}$-PMO (Batch)	583	47.9	27.6	[17]
$Cu_{20}PMO\ Cl^-$ Added (Batch)	593	65.0	40.0	[18]
Cu-Mg/Al	***598***	***59.3***	***48.6***	***This work***

**Includes all reported C_{4+} alcohols*

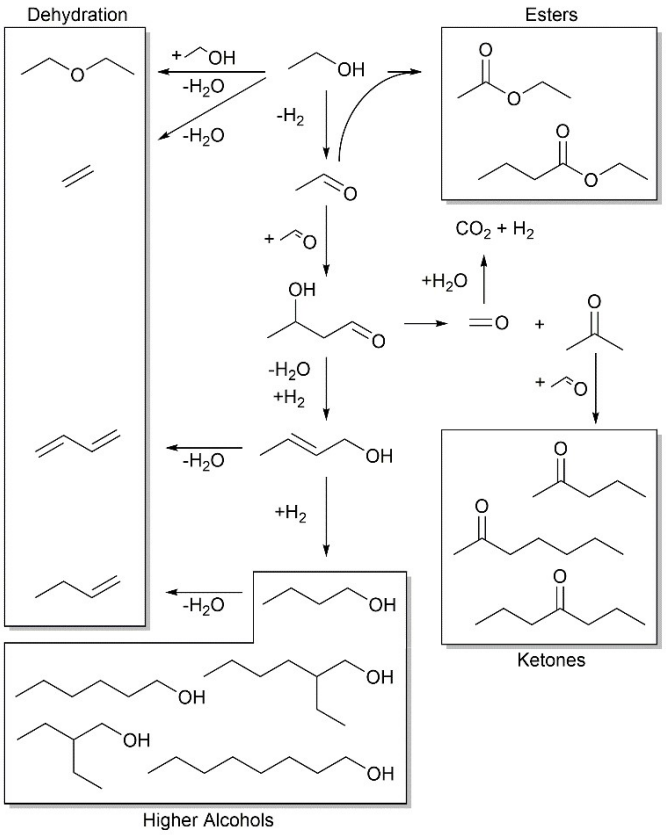

Scheme S1. Reaction pathways showing ethanol coupling to butanol through aldol condensation[19, 20] as well as possible side reactions resulting from dehydration[21, 22], esterification[23-26], and C-C scission to form ketones[8, 25, 27, 28]

Table S2. Ethanol conversion and product distribution for varying copper loadings

Cu Loading	Conv. [mol%]	Carbon Selectivity [mol%]								
		Ethers[a]	EY[b]	Acet[c]	BuOH[d]	C_{6+}OH[e]	Butenes[f]	EtAc[g]	C_{6+}Ester[h]	Ketone[i]
0	33.88	46.09	2.04	0.51	35.06	4.80	8.26	0.59	0.04	0.20
0.025	63.78	2.94	0.20	3.47	51.08	19.35	3.60	1.39	3.54	2.40
0.05	65.67	1.90	0.22	2.97	49.24	24.42	3.87	0.44	6.68	2.42
0.1	65.60	1.24	0.07	3.35	50.19	23.91	2.00	0.26	8.46	3.43
0.25	63.07	1.22	0.02	4.26	31.08	12.13	0.53	3.77	11.85	20.38
0.5	73.34	1.38	0.02	2.94	21.64	11.20	0.63	2.22	3.58	29.19

Reactions Conditions. [a] Diethyl Ether, Butyl Ethyl Ether. [b] Ethylene. [c] Acetaldehyde. [d] 1-Butanol. [e] 1-Hexanol, 2-Ethyl-1-Butanol, 1-Octanol, 2-Ethyl-1-Hexanol. [f] 1-Butene, 2-Butene. [g] Ethyl Acetate. [h] Ethyl butyrate, Butyl acetate, Butyl Butyrate, Hexanoic Acid Ethyl Ester, 2-Ethylbutanoic Acid Ethyl Ester, 2-Ethylhexanoic acid Ethyl Ester, Hexanoic Acid Butyl Ester, Octanoic Acid Butyl Ester, 2-Ethylbutanoic Acid Butyl Ester. [i] Acetone, Methyl Ethyl Ketone, 2-Pentanone, 3-Hexanone, 4-Heptanone, 2-Heptanone, 4-Nonanone

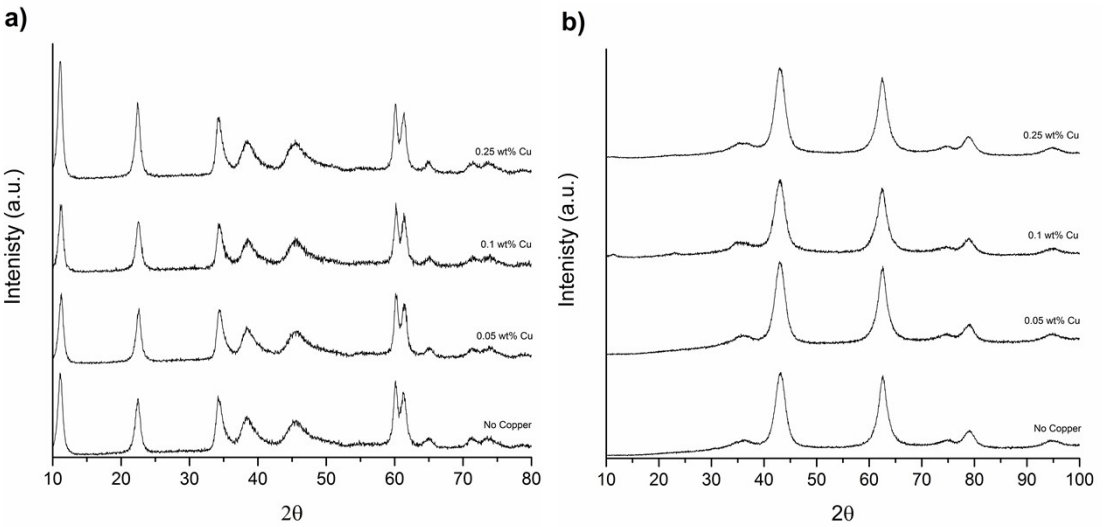

Figure S1. XRD pattern of synthesized MgAl hydrotalcite with different copper loadings (a) before calcination and (b) after calcination

Table S3. Molar Composition of Catalysts determined by ICP Analysis

Nominal Cu Content (wt%)	Molar Composition[a]		
	Cu	Mg	Al
0%	--	3.43	1
0.05%	0.0034	3.42	1
0.1%	0.0072	3.46	1
0.25%	0.0180	3.47	1
0.05%*	0.0034	3.39	1
0.1%*	0.0071	3.40	1
0.25%*	0.0183	3.46	1

***Spent catalyst measured after reaction**

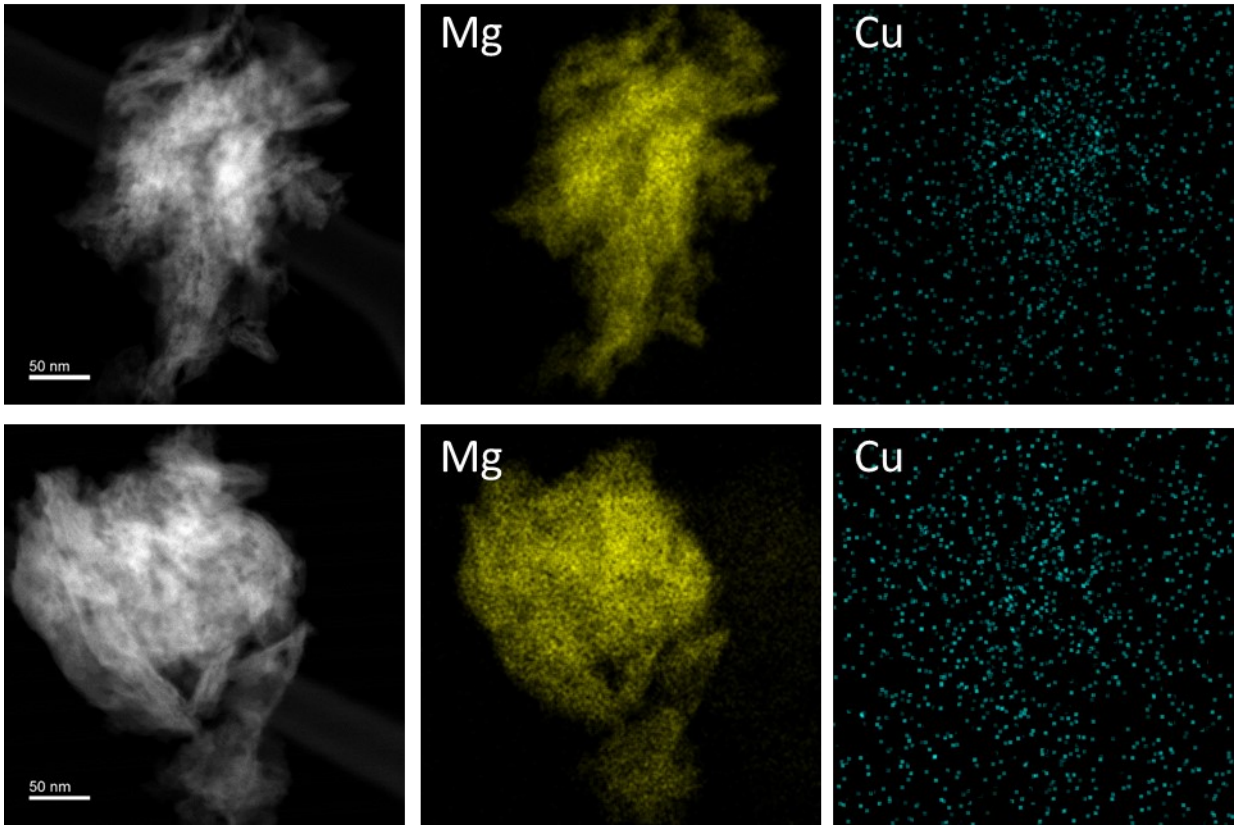

Figure S2. HAADF-STEM and EDX of fresh catalyst of 0.1%Cu (top row) and 0.25% bottom row

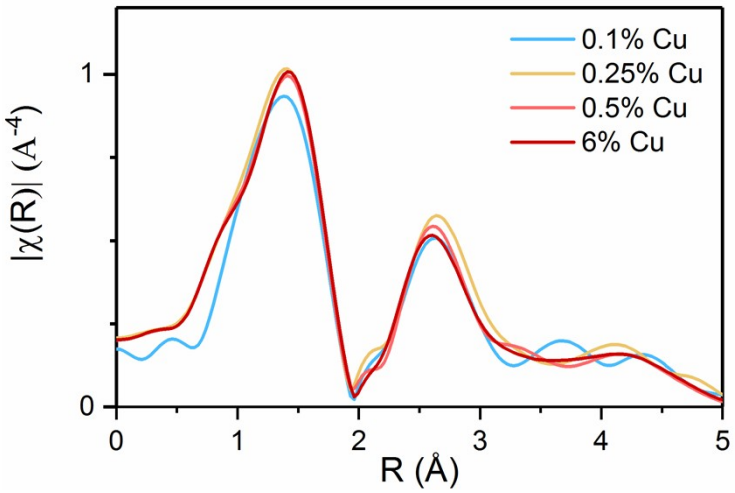

Figure S3. Cu-K-Edge EXAFS (FT magnitude) of catalysts under He flow at 598 K

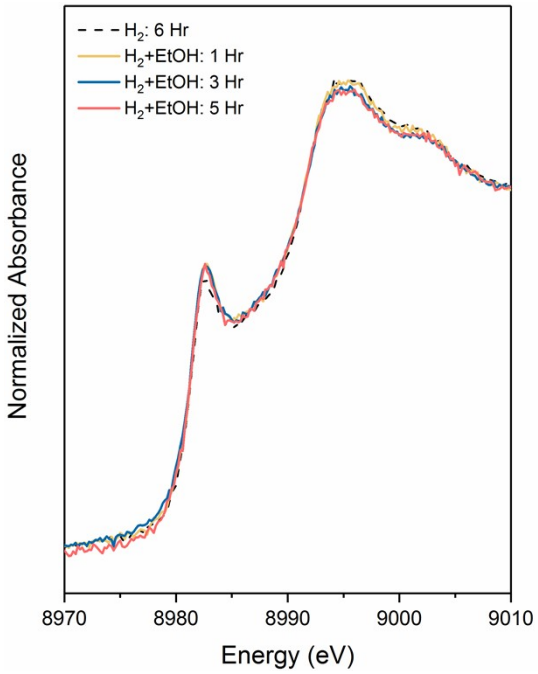

Figure S4. Cu-K-Edge XANES spectra of 0.1%Cu catalyst at 325C showing the stability of the Cu (II) oxidation state after 6 hours H_2 reduction and an additional 5 hours under H_2+EtOH flow *in operando*

Table S4. Fitting EXAFS spectra of catalysts ex-situ and *in operando*

Sample	Shell[a]	CN[b]	r (Å)[c]	DW[d]	Et[f]	
0.1%Cu Ex-Situ	Cu-O	2.829	1.957	0.00584	-1.013	0.009045
	Cu-Mg	4.535	2.954	0.0112	-1.013	
0.1%C *In operando*	Cu-O	1.132	1.861	0.00322	-1.26	0.004078
	Cu-Cu	1.923	2.619	0.02191	-1.26	
0.25%Cu *In Operando*	Cu-O	1.225	1.93	0.00252	2.764	0.005514
	Cu-Cu	9.053	2.5222	0.01926	2.764	
0.1%Cu IW Ex-situ	Cu-O	2.349	1.954	0.00396	0.263	0.025338
	Cu-Mg	2.979	2.968	0.1073	0.263	
0.1%Cu IW *In-operando*	Cu-O	1.603	1.949	0.03217	1.537	0.006596
	Cu-Cu	8.725	2.555	0.02211	1.537	

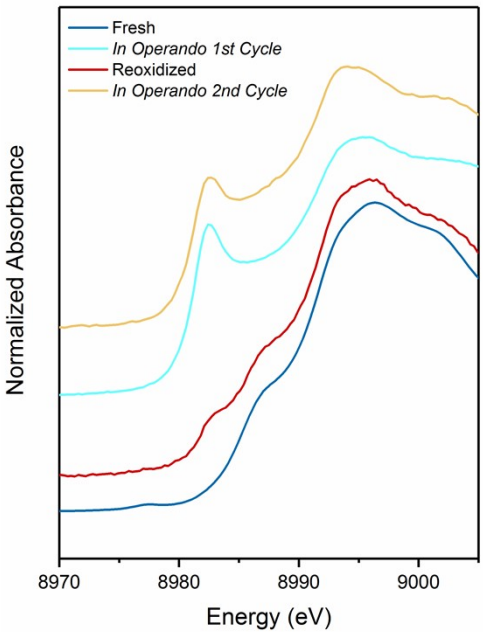

Figure S5. Cu-K-Edge XANES spectra of 0.25%Cu comparing fresh catalyst and reoxidized catalyst exposed to air for 24 hours showing the shift in the shoulder feature of the

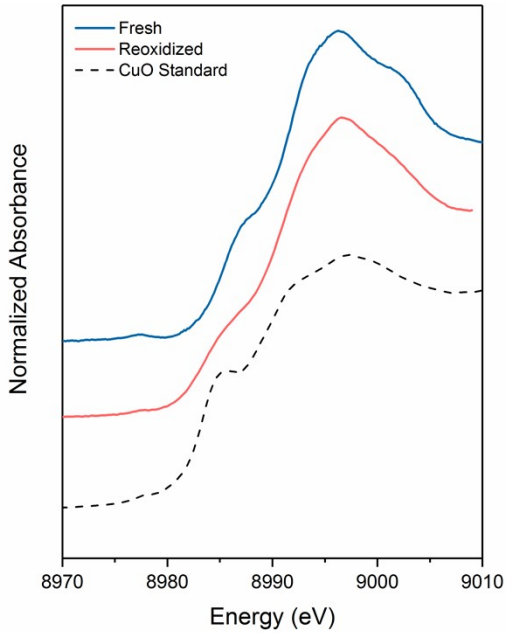

Figure S6. Cu-K-Edge XANES spectra of 0.25%Cu comparing fresh catalyst and reoxidized catalyst exposed to air for 24 hours showing the shift in the shoulder feature of the XANES

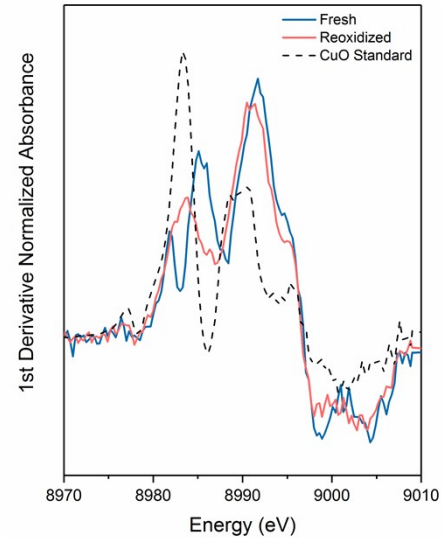

Figure S7. Cu-K-Edge XANES spectra first derivative of 0.25%Cu comparing fresh catalyst and reoxidized catalyst exposed to air for 24 hours showing the decreasing shift in the energy of the Cu^{+2} feature with that of the reoxidized catalyst exhibiting similar alignment to the shoulder feature found in the CuO standard

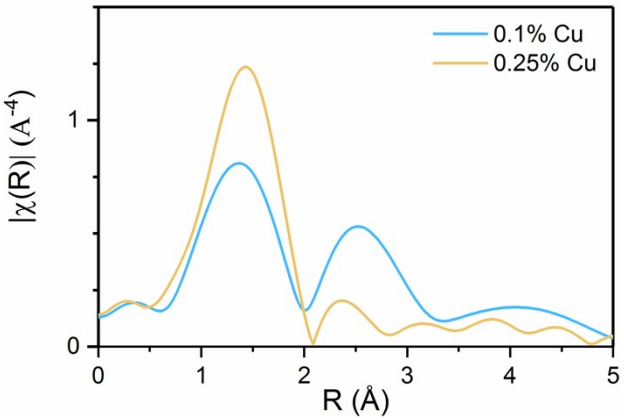

Figure S8 Cu-K-Edge EXAFS spectra comparing the reoxidized 0.1%Cu and 0.25%Cu catalyst showing the lower Cu-O shell for 0.1%Cu signaling a more reduced character as well as a stronger Cu-Mg peak demonstrating the reintegration of the copper into support structure. The 0.25%Cu catalyst is more oxidized but the absence of other peaks indicate that the copper has not been reintegrated.

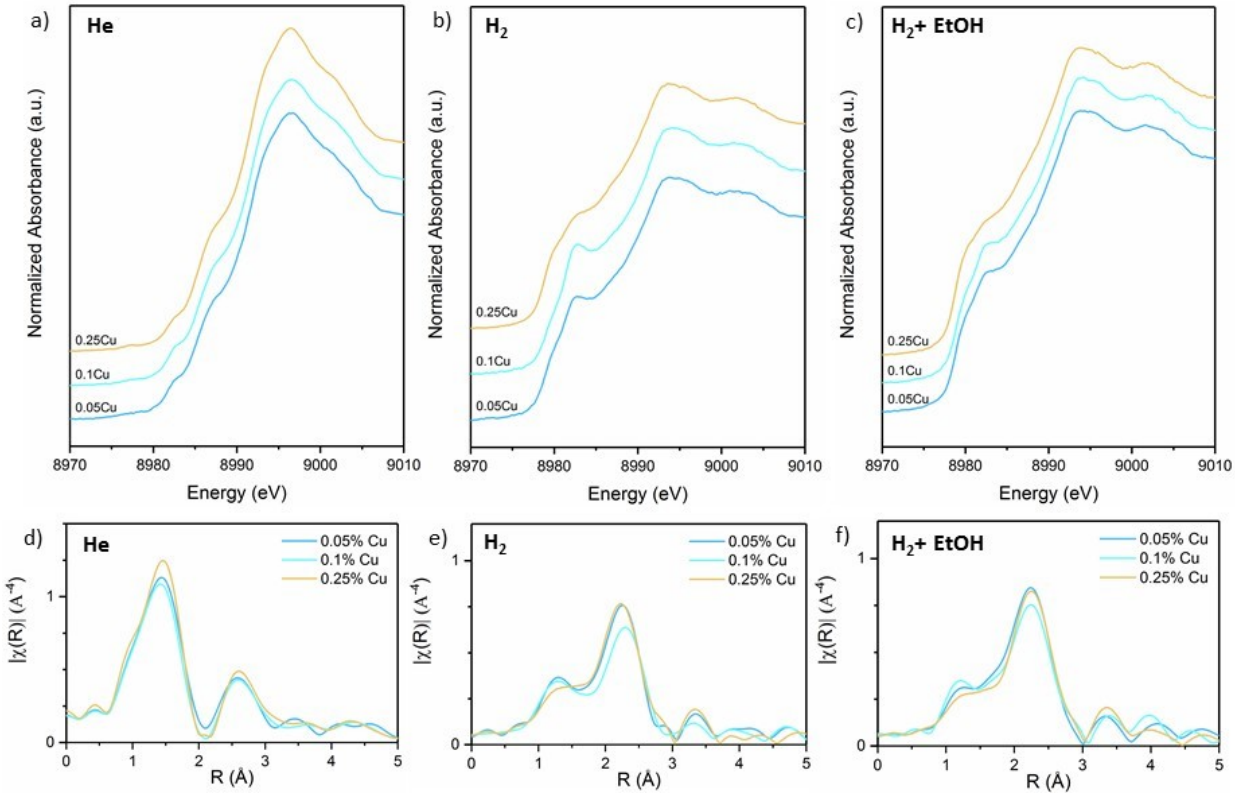

Figure S9. Cu K-Edge XANES (a-c) and EXAFS (d-f) comparing different concentrations of impregnated Cu/HT catalyst in respective He, H_2, and H_2+EtOH flows at 598 C

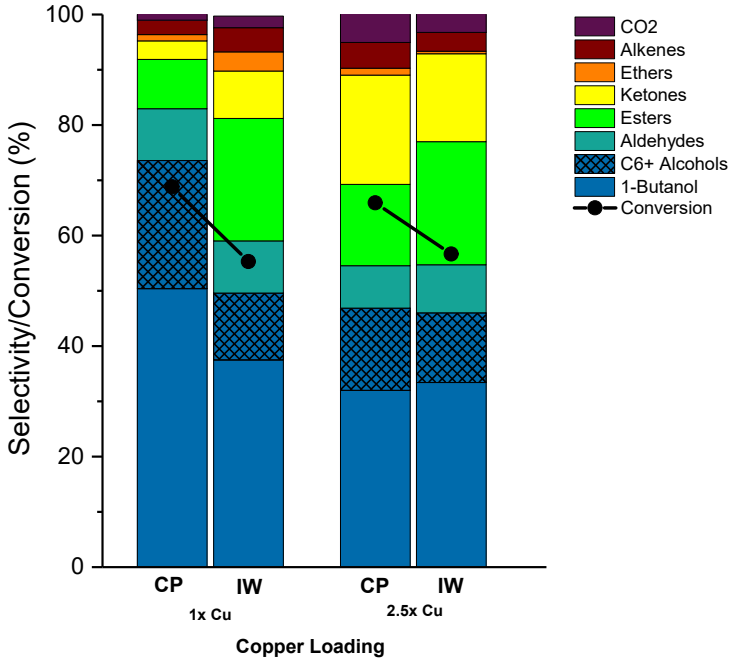

Figure S10. Comparison of ethanol conversion and selectivity of impregnated and coprecipitated catalysts at 325 C, 300 PSI H_2, 0.2 $WHSV^{-1}$

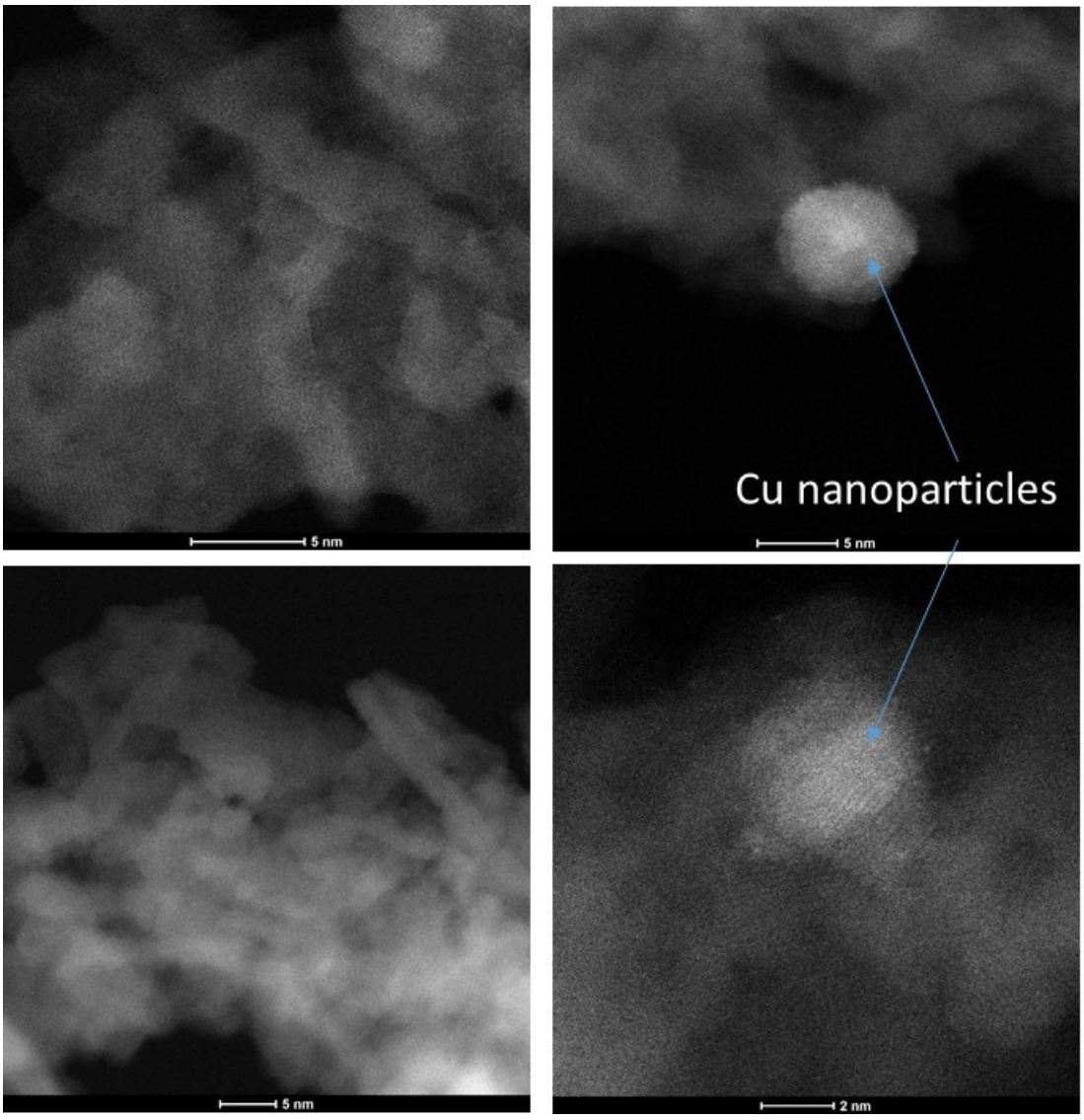

Figure S11. HAADF-STEM of spent 0.1%Cu impregnated catalyst after >60 hour time on stream showing the presence of copper nanoparticles indicating the sintering that occurs during the reaction

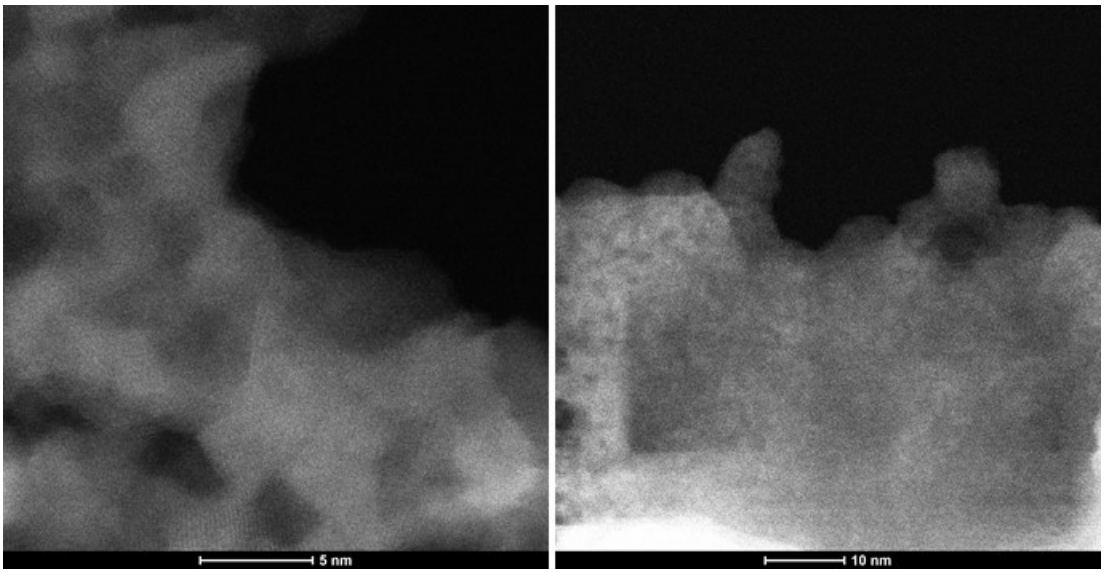

Figure S12. HAADF-STEM of fresh 0.1%Cu impregnated catalyst showing well-dispersed copper

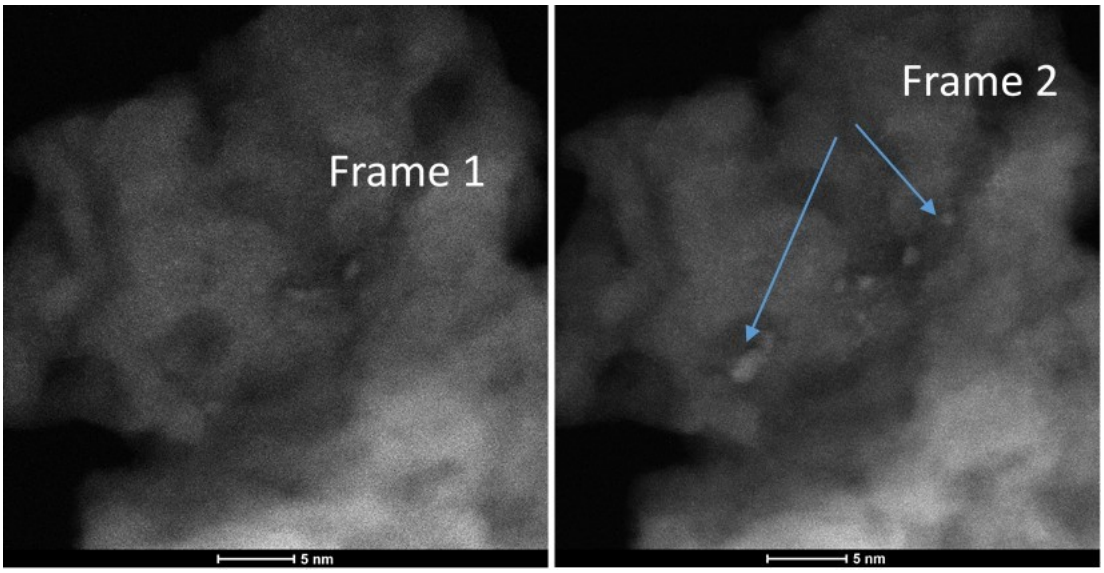

Figure S13. HAADF-STEM of fresh 0.1%Cu impregnated catalyst showing susceptibility to copper sintering into approximately 2nm nanoparticles under electron beam that is visible in real-time

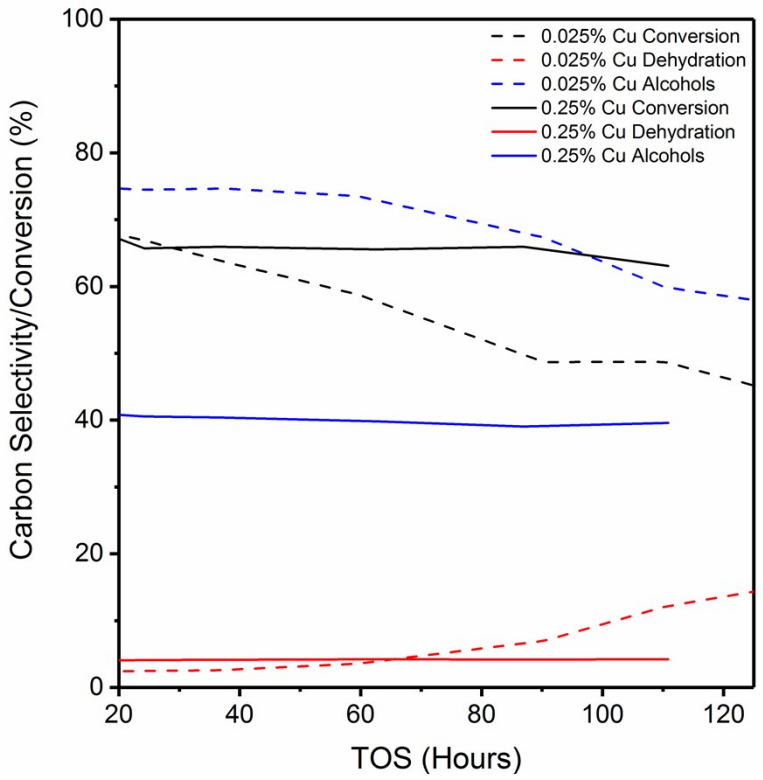

Figure S14. Extended catalyst testing at 598 K temperature, 300 psig pressure H_2, 0.2 hr-1 weight hourly space velocity (WHSV) for 0.25 and 0.025% Cu loaded catalyst

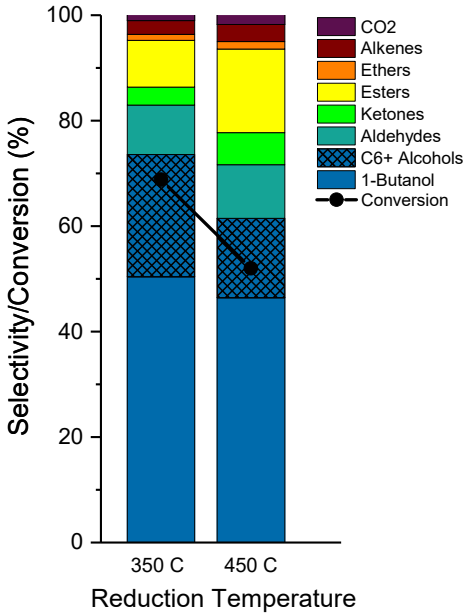

Figure S15. Comparison of ethanol conversion and selectivity of 0.1%Cu co-precipitated catalyst with different pre-reduction temperatures

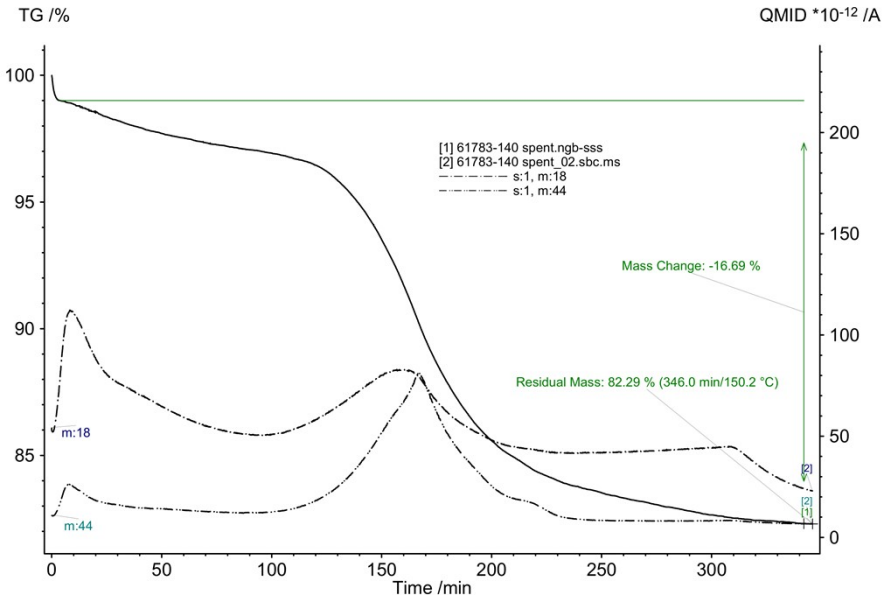

Figure S16. Thermogravimetric analysis of spent 0.1%Cu catalyst after deactivation

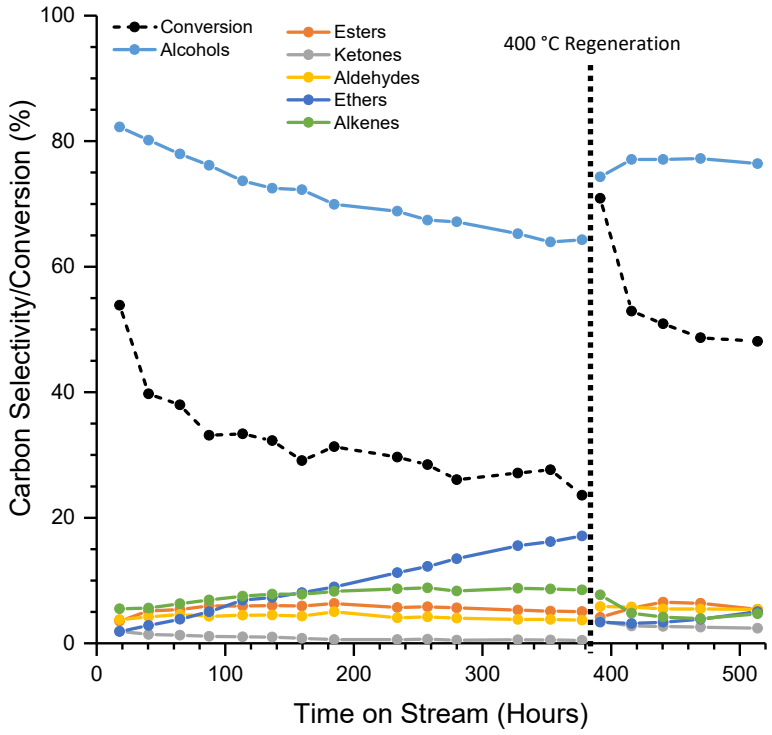

Figure S17. Time on stream graph showing carbon selectivity and conversion of the catalyst

Technoeconomic Evaluation

A technoeconomic analysis was completed for a conceptual process to convert 95 wt% ethanol/5 wt% water mixture into chemical grade n-butanol plus a 1-hexene co-product. A simplified block flow diagram of the process is illustrated in Figure S16. The ethanol conversion process has a single reactor with multiple catalyst beds using two catalysts types. A hydrotalcite-based catalyst, described in the main text, was used for coupling ethanol to produce n-butanol (Guerbet reactor), and a second proprietary catalyst for hydrogenation of by-product aldehydes and esters back into alcohols to facilitate separation and recycling downstream. The gas stream into the reactor is maintained with a hydrogen concentration of 61 mole percent to improve selectivity to desired products and to minimize coke formation on the catalyst.

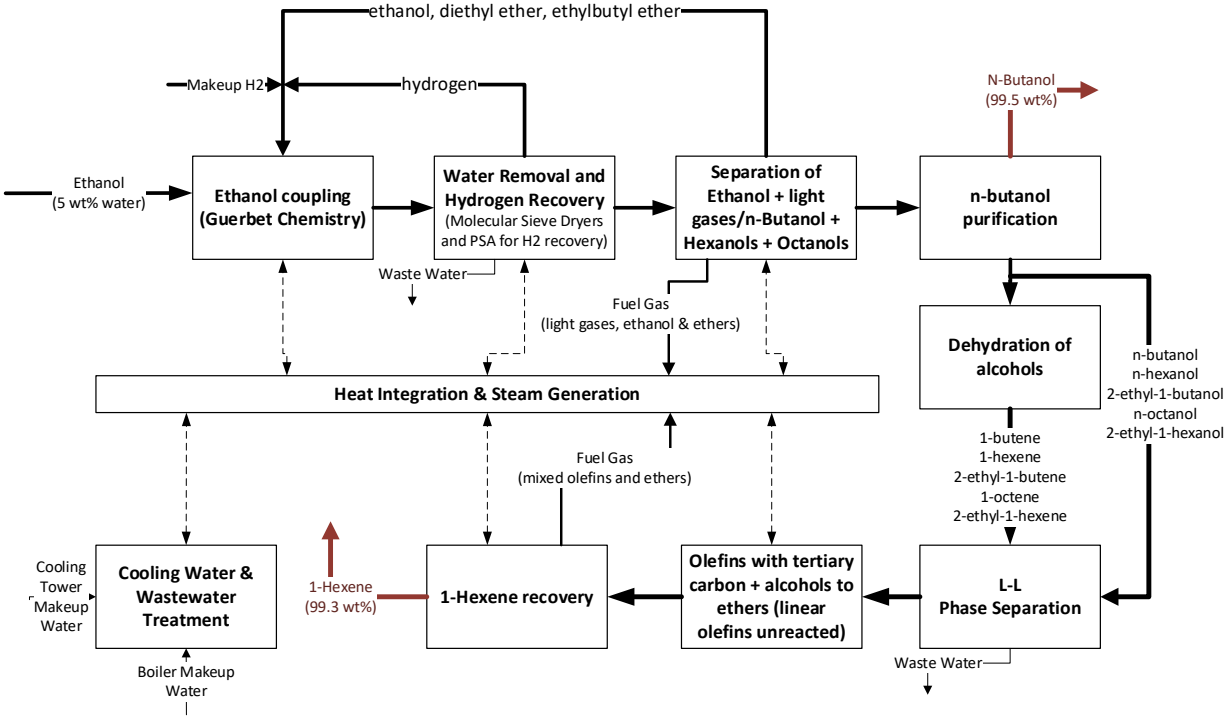

Figure S18 Block flow diagram developed from the base case techno economic analysis of the ethanol to n-butanol process with a 1-hexene co-product.

The effluent from the Guerbet reactor is a mixture of alcohols, water, ethers and hydrogen. The mixture of oxygenates is difficult to separate because of azeotrope formation. It was outside the scope of the project to develop a process to break the azeotrope, therefore water was removed from both process streams using hydrophilic molecular sieve units for each phase. The recovered hydrogen is recompressed and recycled to the Guerbet reactor, and the impurities back flushed from the PSA are recompressed and recycled or purged to fuel gas combustion.

After removing the water and hydrogen, distillation is used to separate ethanol and other light components (overhead) from the desired heavier C_{4+} components (bottom). The overhead from the column is cooled and light gases stripped from the ethanol. A purge stream was used to limit the concentration of non-separable gases.

The bottom stream from the ethanol splitter column was distilled again to recover a high-purity (> 99.5 wt.%) n-butanol product collected in the overhead stream. The bottom flow from the butanol splitter column is a mixture of n-hexanol, 2-ethyl-1-butanol, n-octanol, 2-ethyl-1-hexanol, and dibutyl ether. 1-hexene was a desired co-product to improve process economics. However, n-hexanol (a precursor for 1-hexene via dehydration) does not easily separate from the other oxygenates in the stream because of azeotrope formation between n-hexanol and 2-ethyl-1-butanol. Instead, part of the mixed alcohol stream was dehydrated with alumina, producing olefins and water which were mixed back with the remaining alcohols. The mixture was cooled and water removed from the 2-phase liquid in a decanter vessel. The remaining mixture of alcohols and olefins were then reacted over an Amberlyst-15 catalyst bed at 90 °F to react the olefins with a tertiary carbon atom (2-ethyl-1-butene and 2-ethyl-1-hexene) with alcohols to form

a mixture of higher-boiling point ether compounds; the linear olefins (1-hexene and 1-octene) do not react with alcohols and pass through unchanged. The reaction is equilibrium limited.

For modeling purposes, the 2-ethyl-1-butene was eliminated by recycling the unreacted residuals, which allowed the 1-hexene to be easily separated from the remaining compounds by simple distillation. This conceptual method is based on the well-known process for making MTBE and ETBE by reacting methanol or ethanol with isobutene, an olefin with a tertiary unsaturated carbon. The reaction and separation could be done using reactive distillation to drive the reaction to completion. The mixture of heavier, unreacted alcohols, ethers and higher boiling point olefins were blended with fuel gas for steam generation and process heat.

The process economics were estimated using an Excel spreadsheet-based cost model that has been used in numerous studies. The cost model results, based on 2016 US dollars, are summarized in Table S5.

The Guerbet catalyst was estimated to cost $6/lb based on the catalyst costing tool recently developed by the Department of Energy's National Renewable Energy Laboratory and Pacific Northwest National Laboratory under the ChemCatBio (https://catcost.chemcatbio.org). At the assumed one-year catalyst lifetime and experimentally determined WHSV of 0.2 hr^{-1}, a 100% increase in the catalyst cost resulted in only a 4% increase in MBSP. The MBSP is insensitive to Guerbet catalyst lifetime, assuming it lasts at least 6 months. Shorter catalyst lifetimes however would incur significant CAPEX and OPEX costs associated with installation of swing reactors and catalyst regeneration. Doubling the lifetime of this catalyst had about 2% decrease in MBSP. The MBSP is more sensitive to the higher cost hydration catalyst in the last section of the Guerbet reactor.

Initially, recovery of a pure n-butanol product proved difficult to achieve in the process model because of the presence of esters that formed azeotrope mixtures. A proprietary catalyst capable of converting the aldehydes and esters back to alcohols without impacting the desired butanol products was developed and added to the final bed section of the Guerbet reactor. The cost of this catalyst was estimated to be $54/lb with an assumed lifetime of 2 years. The higher cost of this catalyst makes the MBSP have higher sensitivity to the catalyst lifetime, especially for lifetimes less than 1 year. A 50% decrease in its lifetime increased the MBSP by about 5%.

The ethanol cost contributes 98% of the $0.55/lb MBSP when 1-hexene can be sold for $0.80/lb. The sale of 1-hexene co-product decreases the MBSP by about 10 cents per pound (20%). Since ethanol is responsible for nearly all of the cost to make n-butanol, the MBSP is extremely sensitive to this cost with an increase in ethanol changing the MBSP by the same relative amount. A ±25% change in the 1-hexene market value has less than a 5% impact on the MBSP, and a 50% change in CAPEX has only a 3% impact on MBSP.

Table S5. Model information for estimating MBSP using an ethanol feedstock with a 1-hexene co-product. The first column comes from the base case for this paper. The second column is the same process configuration with a lower per pass conversion. The yield of products is slightly less for the lower per pass conversion case because the unconverted ethanol is recycled. The minimum butanol selling price increases by about 7% for the lower per pass conversion case due to increased equipment sizes, decreased co-product yield and higher power consumption related primarily to recycle compressors.

	60% single-pass conversion	39% single pass conversion
Ethanol (95%) Cost, $/gal	2.00	2.00
Ethanol Feed Rate (incl. water), gph	7161	7161
n-butanol (99.5 wt%), lb/hr	25545	25432
1-hexene, lb/hr	3388	2954
Minimum n-Butanol Selling Price, $/lb	0.55	0.59
1-hexene value, $/lb	0.807	0.807
Guerbet Reactor, WHSV, /hr	0.2	0.2
Temperature, F	617	617
Pressure, psia	296	296
Hydrogenation Bed, WHSV, /hr	1.0	1.0
Ethanol Conversion per pass, %	60	39
Carbon (from ethanol) converted to n-butanol, %	69.1	68.7
Carbon (from ethanol) converted to 1-hexene, %	12.1	10.6
CAPEX (Total Capital Investment), mm$	69.2	91.2
OPEX (variable and fixed), mm$/yr	111	118
Power consumption, MW	3.0	3.6

References:

1. I.-C. Marcu, N. Tanchoux, F. Fajula and D. Tichit, *Catalysis Letters*, 2013, **143**, 23-30.
2. I.-C. Marcu, D. Tichit, F. Fajula and N. Tanchoux, *Catalysis Today*, 2009, **147**, 231-238.
3. K. Kourtakis, R. Ozer and M. B. D'Amore, *Journal*, 2012.
4. T. L. Jordison, C. T. Lira and D. J. Miller, *Industrial & Engineering Chemistry Research*, 2015, **54**, 10991-11000.
5. K. K. Ramasamy, M. Gray, H. Job, C. Smith and Y. Wang, *Catalysis Today*, 2016, **269**, 82-87.
6. M. León, E. Díaz and S. Ordóñez, *Catalysis Today*, 2011, **164**, 436-442.
7. D. L. Carvalho, L. E. P. Borges, L. G. Appel, P. Ramírez de la Piscina and N. Homs, *Catalysis Today*, 2013, **213**, 115-121.
8. J. I. Di Cosimo, Apesteguı, C. R.́a, M. J. L. Ginés and E. Iglesia, *Journal of Catalysis*, 2000, **190**, 261-275.
9. Z. Sun, A. Couto Vasconcelos, G. Bottari, M. C. A. Stuart, G. Bonura, C. Cannilla, F. Frusteri and K. Barta, *ACS Sustainable Chemistry & Engineering*, 2016, DOI: 10.1021/acssuschemeng.6b02494.
10. D. Stošić, F. Hosoglu, S. Bennici, A. Travert, M. Capron, F. Dumeignil, J. L. Couturier, J. L. Dubois and A. Auroux, *Catalysis Communications*, 2017, **89**, 14-18.
11. J. Pang, M. Zheng, L. He, L. Li, X. Pan, A. Wang, X. Wang and T. Zhang, *Journal of Catalysis*, 2016, **344**, 184-193.
12. J. H. Earley, R. A. Bourne, M. J. Watson and M. Poliakoff, *Green Chemistry*, 2015, **17**, 3018-3025.
13. D. Jiang, X. Wu, J. Mao, J. Ni and X. Li, *Chemical Communications*, 2016, **52**, 13749-13752.
14. N. M. Eagan, B. M. Moore, D. J. McClelland, A. M. Wittrig, E. Canales, M. P. Lanci and G. W. Huber, *Green Chemistry*, 2019, **21**, 3300-3318.
15. D. D. Petrolini, N. Eagan, M. R. Ball, S. P. Burt, I. Hermans, G. W. Huber, J. A. Dumesic and L. Martins, *Catalysis Science & Technology*, 2019, **9**, 2032-2042.

16. N. V. Vlasenko, P. I. Kyriienko, K. V. Valihura, G. R. Kosmambetova, S. O. Soloviev and P. E. Strizhak, *ACS Omega*, 2019, **4**, 21469-21476.
17. Z. Sun, A. Couto Vasconcelos, G. Bottari, M. C. A. Stuart, G. Bonura, C. Cannilla, F. Frusteri and K. Barta, *ACS Sustainable Chemistry & Engineering*, 2017, **5**, 1738-1746.
18. J. A. Barrett, Z. R. Jones, C. Stickelmaier, N. Schopp and P. C. Ford, *ACS Sustainable Chemistry & Engineering*, 2018, **6**, 15119-15126.
19. A. Galadima and O. Muraza, *Industrial & Engineering Chemistry Research*, 2015, **54**, 7181-7194.
20. W. Xianyuan, F. Geqian, T. Yuqin, J. Dahao, L. Zhe, L. Wenhua, L. Liu, T. Pengxiang, W. Hongjing, N. Jun and L. Xiaonian, *ChemSusChem*, 2018, **11**, 71-85.
21. J. F. DeWilde, C. J. Czopinski and A. Bhan, *ACS Catalysis*, 2014, **4**, 4425-4433.
22. W. Knaeble and E. Iglesia, *The Journal of Physical Chemistry C*, 2016, **120**, 3371-3389.
23. Z. Federica, S. Nicola and R. Nicoletta, *ChemCatChem*, 2018, **10**, 1526-1535.
24. D. D. Petrolini, W. H. Cassinelli, C. A. Pereira, E. A. Urquieta-González, C. V. Santilli and L. Martins, *RSC Advances*, 2019, **9**, 3294-3302.
25. S. Wang, K. Goulas and E. Iglesia, *Journal of Catalysis*, 2016, **340**, 302-320.
26. K. Inui, T. Kurabayashi and S. Sato, *Applied Catalysis A: General*, 2002, **237**, 53-61.
27. M. J. L. Gines and E. Iglesia, *Journal of Catalysis*, 1998, **176**, 155-172.
28. M. Neurock, Z. Tao, A. Chemburkar, D. Hibbitts and E. Iglesia, *Faraday Discussions*, 2016, DOI: 10.1039/C6FD00226A.